First Order Alignment Transition in an Interfaced Active Nematic Fluid

Olga Bantysh,[1,2] Berta Martínez-Prat,[1,2] Jyothishraj Nambisan,[3] Alberto Fernández-Nieves,[3,4,5] Francesc Sagués,[1,2,*] and Jordi Ignés-Mullol[1,2,†]

[1]*Department of Materials Science and Physical Chemistry, Universitat de Barcelona, 08028 Barcelona, Spain*
[2]*Institute of Nanoscience and Nanotechnology, IN2UB, Universitat de Barcelona, 08028 Barcelona, Spain*
[3]*Department of Condensed Matter Physics, Universitat de Barcelona, 08028 Barcelona, Spain*
[4]*Institute of Complex Systems, UBICS, Universitat de Barcelona, 08028 Barcelona, Spain*
[5]*ICREA-Institucio Catalana de Recerca i Estudis Avançats, Barcelona, Spain*

(Received 13 June 2023; revised 5 October 2023; accepted 18 April 2024; published 29 May 2024)

We investigate experimentally the dynamic phase transition of a two-dimensional active nematic layer interfaced with a passive liquid crystal. Under a temperature ramp that leads to the transition of the passive liquid into a highly anisotropic lamellar smectic-*A* phase, and in the presence of a magnetic field, the coupled active nematic reorganizes its flow and orientational patterns from the turbulent into a quasilaminar regime aligned perpendicularly to the field. Remarkably, while the phase transition of the passive fluid is known to be continuous, or second order, our observations reveal intermittent dynamics of the order parameter and the coexistence of aligned and turbulent regions in the active nematic, a signature of discontinuous, or first order, phase transitions, similar to what is known to occur in relation to flocking in dry active matter. Our results suggest that alignment transitions in active systems are intrinsically discontinuous, regardless of the symmetry and momentum-damping mechanisms.

DOI: 10.1103/PhysRevLett.132.228302

The concept of phase transition is ubiquitous in condensed matter physics. It is also commonplace in active matter [1–3] where, for instance, the concept of motility induced phase separation [4] has become a paradigm to explain the aggregation of self-motile colloids in the absence of attractive forces. By referring to dry active systems, the spontaneous assembling of flocks that coexist with a rarefied phase can be similarly understood as a phase transition that occurs in dense assemblies of moving units that interact through noisy rules [5–7]. The nature of this transition has been much debated. The current consensus is that it is first order, featuring phase coexistence and strong finite size effects [7–9]. However, a similar assessment has not been reached in the context of active fluids or wet active matter, which encompass the vast majority of biological systems, such as bacteria colonies, cell tissues, or suspensions of cytoskeleton proteins.

Indeed, while phases have often been identified in the study of active fluids [10–13], phase transitions have not been similarly pinpointed. This is remarkable since the constituents of some of their more celebrated experimental realizations display distinctive orientational symmetries, thus allowing the observed textures to be characterized in terms of standard order parameters. Recently, experiments have demonstrated that the kinetics and morphology of a phase-separating polymer mixture can be changed if there is coupling with a kinesin-tubulin active gel [14], which can further decrease the critical temperature of a demixing DNA solution [15]. Moreover, numerical simulations [16,17] have studied the phase separation of binary liquid mixtures in which one of the components is active. None of these studies considers the fundamental issue of a genuine phase transition in a single-component active liquid. This is required to assess whether alignment transitions, a trademark of active systems, are intrinsically discontinuous, or whether this depends on their symmetry and momentum-damping mechanisms.

In this Letter, we study the alignment transition of an active nematic (AN) layer of bundled tubulin microtubules cross-linked with kinesin motors prepared at the water-oil interface [18,19]. While adenosine triphosphate (ATP) concentration controls the chaotic flows in the typical unconstrained preparations [20–22], here we take advantage of the known coupling between AN flows and the oil viscosity [23–25]. Using a thermotropic liquid crystal as the oil phase, the interface rheology can be continuously switched between isotropic (nematic oil phase) and strongly anisotropic (smectic oil phase), prompting AN flows to transit from turbulent to aligned along the easy-flow direction set by the anisotropic interface viscosity [24,26]. By controlling this process with a precise temperature ramp, we have detected intermittency and spatial coexistence between the two phases, a clear signature of discontinuous flow alignment transitions.

Samples are enclosed by a cylindrical copper oven placed in the 25-mm-wide cylindrical cavity of a 1T Halbach array formed by eight permanent magnets (Bunting Magnetics Europe Ltd.), where the magnetic

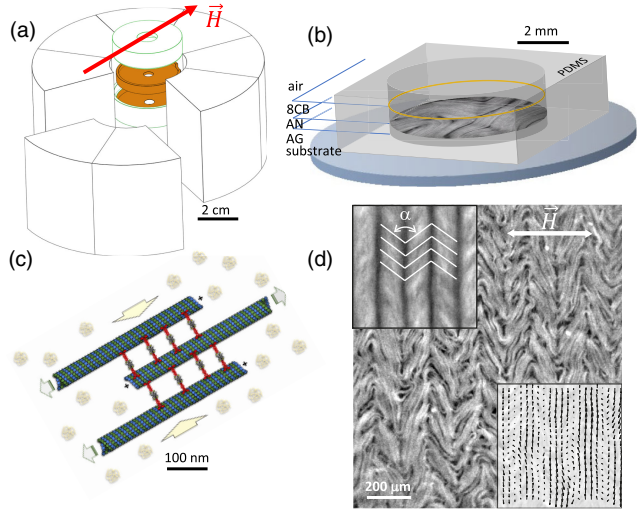

FIG. 1. (a) Sketch of the setup. Two of the eight magnets that form the 1 T Halbach array are shifted to reveal the copper disks (in orange in the sketch) that form thermostatic oven holding the sample. (b) Experimental open cell where the AN is formed at the aqueous (active gel, AG)–liquid crystal (8CB) interface. (c) Depletion forces and active cross-linking lead to the formation of the extensile active fluorescent filaments. (d) Aligned AN flows upon transition of 8CB into the Sm*A* phase (see Supplemental Material, Movie S1 [27]). Top left inset: time-averaged fluorescence images. The active filaments organize in a chevron-like pattern (depicted by the white segments that zigzag with an angle α). Bottom right inset: instantaneous velocity field. The orientation of the magnetic field, $\vec{H}$, is depicted with arrows.

field is homogeneous in a region larger than the field of view [Fig. 1(a)]. The copper cell is equipped with heating elements (Thorlabs HT19R) and a PT100 temperature sensor (Thorlabs TH100PT), both driven by a RKC-HA400 controller that ensures a temperature stability of 0.01 °C. The inner windows of the copper oven are sealed with sapphire plates to optimize thermal contact with the sample and to minimize in-plane temperature gradients across the aperture, while the outer windows are closed with glass plates for optimal thermal insulation. The active nematic layer forms at the interface between the aqueous subphase and the thermotropic liquid crystal octyl-cyanobiphenyl (8CB). The liquids are placed inside a 6 mm-wide circular pool made from a polydimethyl siloxane elastomer that is glued to a coverslip glass, which has been previously coated with a repulsive polyacrylamide brush [24] [Fig. 1(b)].

A small volume (1 μL) of the kinesin-tubulin active mixture is placed on top of the hydrophilic glass, where it quickly spreads. The active material is prepared as described previously, with the composition detailed in Supplemental Material, Table S1 [27]. The aqueous active mixture is readily covered by 35 μL of 8CB, which forms a layer $\simeq$1 mm thick on top of the much thinner active layer. The presence in the aqueous phase of the surfactant Pluronic-F127, used to protect the proteins from the oil interface, also favors the alignment of mesogen molecules parallel to the oil-aqueous interface, while remaining perpendicular to the oil-air interface. A combination of active flows and depletion forces [Fig. 1(c)] lead to the accumulation of the active filaments on the water-oil interface, forming the quasi-two-dimensional AN film that will be the object of our study [19]. Labeling of a fraction of the tubulin molecules allows observation of the filamentous material by means of fluorescence microscopy.

While 8CB is in the low-anisotropy nematic phase, the AN appearance does not differ measurably from the so-called active turbulent regime, characterized by chaotic flows and a proliferation of $\pm 1/2$ defects moving in random directions [19]. Lowering the temperature below ca. 33.5 °C leads to 8CB transitioning into the highly anisotropic smectic-*A* (Sm*A*) phase, in a process that is known to be continuous, or second order [28]. 8CB molecules align with the magnetic field $\vec{H}$ and organize in layers perpendicular both to the field and to the interface (bookshelf configuration) [24]. While layer-sliding allows 8CB to behave as a viscous fluid in one direction, flows perpendicular to the layers are severely hindered. This determines an easy-flow direction perpendicular to the field. Active flows, hydrodynamically coupled to the anisotropic oil interface, adapt to the new environment, and become pseudolaminar, with a velocity field that becomes perpendicular to the magnetic field and develops a pattern of alternating antiparallel flow lanes [Fig. 1(d)]. The latter appear dark in time-averaged fluorescence micrograph, as they concentrate the self-propelled AN defects. Simultaneously, the active filaments reorganize into chevronlike patterns, whose vertices are aligned with the flow [Fig. 1(d)], and whose zigzag angle α becomes smaller for higher activities (ATP concentrations).

We then analyze the AN alignment transition as the temperature is slowly and spatially homogeneously decreased from 33.60 °C (8CB in nematic phase, AN in turbulent regime) down to 33.40 °C (8CB in Sm*A* phase, AN in aligned state). At high temperatures, both the AN orientational and flow fields are isotropic [Figs. 2(a) and 2(d)]. As the temperature is decreased, the alignment transition spans a range of about 0.10 °C, from the first signatures of anisotropic velocity distribution at $T = 33.50$ °C (Supplemental Material, Fig. S1 [27]) until the final steady state is reached at $T = 33.40$ °C, where active flows are, on average, perpendicular to $\vec{H}$ and active filaments develop chevronlike patterns in their orientational field [Figs. 2(c) and 2(f)]. Emergence of anisotropy in the latter is slightly delayed with respect to the velocity field, and is only detectable for $T \leq 33.47$°C (see Supplemental Material, Fig. S1 [27]).

To better quantify the ordering transition we define a scalar order parameter for the velocity field, $\psi_v = 2\sin^2(\theta_{\hat{v},\hat{H}}) - 1$, where $\theta_{\hat{v},\hat{H}}$ is the angle between the local

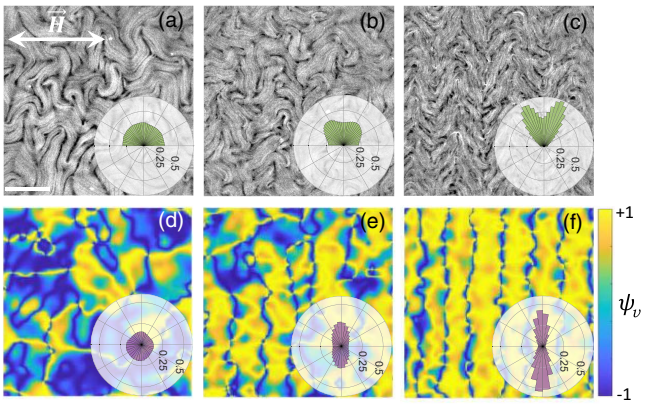

FIG. 2. Alignment transition of the active nematic. The magnetic field $\vec{H}$ is along the horizontal direction. Panels correspond to $T = 33.60\,^{\circ}\mathrm{C}$ [(a),(d) turbulent phase], $T = 33.47\,^{\circ}\mathrm{C}$ [(b),(e) transition], and $T = 33.40\,^{\circ}\mathrm{C}$ [(c),(f) aligned phase]. Panels (a)–(c) are instantaneous fluorescence micrographs. The insets are the distribution of director field orientations accumulated for the duration of the experiment. Panels (d)–(f) are plots of the corresponding instantaneous order parameter of velocity orientations (see Supplemental Material, Movie S2 [27]). The insets represent the distribution of velocity orientations accumulated for the duration of the experiment. Labels in all insets indicate the relative presence of each orientations. Scale bar, 300 μm.

AN velocity and the magnetic field. While ψ_v is randomly distributed with a mean value around 0 in the turbulent regime [Fig. 2(d)], its mean value increases as AN enters into the transition region [Fig. 2(e)], and it is maximum in the aligned state [Fig. 2(f)]. This parameter maps the flow lanes that characterize the aligned state and intermittently emerge during the transition. To monitor the evolution from the disordered to the aligned state, we perform a statistical analysis of ψ_v at constant temperature. First we take a spatial average of the instantaneous distribution of ψ_v, denoted $\bar{\psi}_{v,t}$, and then compute the time average $\bar{\psi}_v$ and its standard deviation over 480 s. The result is plotted in Fig. 3 for different temperatures during a stepwise ramp. We find that $\bar{\psi}_v$ is close to zero in the turbulent regime, consistent with a statistically isotropic distribution of orientations, and about 0.55 in the aligned regime.

For experimental conditions where velocimetry may not be accurate enough, we have considered an alternative order parameter, $\psi_n = 2\sin^2(\theta_{\hat{n},\hat{H}}) - 1$, where $\theta_{\hat{n},\hat{H}}$ now refers to the angle between the local director field of the AN and the magnetic field. In general ψ_v allows us to follow the alignment transition more clearly. For instance, we observe that early stages are first picked up by $\bar{\psi}_v$, and that $\bar{\psi}_n$ reaches a somewhat lower steady-state value in the aligned state (see Supplemental Material, Fig. S2 [27]). This is expected since $\bar{\psi}_n$ depends on the angle α spanned by the chevron segments [Fig. 1(d)], which decreases with activity. For different experimental realizations under the same nominal conditions, the value of the order parameters can change about 5%, likely due to small imprecisions in the concentration of ATP.

The correlation between the onset of the alignment transition in the AN layer and the N-SmA phase boundary in 8CB can be assessed using a temperature gradient created by unsealing the bottom glass windows of the oven. Although the magnitude of the gradient is not known, this enables the simultaneous observation, within the field of view, of all regimes described during the alignment transition. In Supplemental Material, Fig. S3a [27], the sample is rotated so that the N-SmA interface, which will be perpendicular to the local temperature gradient, is also perpendicular to the magnetic field. By imaging in polarization mode, we assessed the state of the 8CB layer along the gradient, revealing the precise location of the N-SmA phase boundary in the field of view. We then measured $\bar{\psi}_n$ as a function of the position along the gradient (Supplemental Material, Fig. S3b [27]), and found that the steepest change corresponds to the location of the N-SmA phase boundary. Consequently, in our stepwise temperature ramp experiments (Fig. 3 and Supplemental Material, S2 [27]) we define T_c as the temperature with the steepest change in the order parameters. We did not observe evidence of hysteresis when comparing upward and downward temperature ramps, with T_c taking values that differ $\pm 0.01\,^{\circ}\mathrm{C}$ at most. Combining data for experiments with both upward and downward ramps, and plotting a normalized $\bar{\psi}_n$ that uses the upper (aligned) and lower (turbulent) values, versus $T - T_c$, we find that all data follow the same trend (see Supplemental Material, Fig. S4 [27]).

As evidenced in Figs. 3 and Supplemental Material, S2 [27], the order parameters feature significant fluctuations about their mean values at constant temperature, exhibiting the highest amplitude in the transition region. An analysis of the origin of these temporal fluctuations reveals

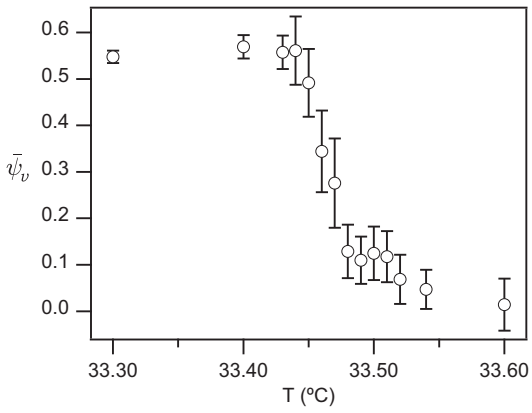

FIG. 3. Evolution of the velocity order parameter of the active nematic averaged in space and time $\bar{\psi}_v$ as defined in the text. Temperature is changed stepwise from $33.60\,^{\circ}\mathrm{C}$ down to $33.30\,^{\circ}\mathrm{C}$. Error bars correspond to the standard deviation of the mean order parameter at each temperature.

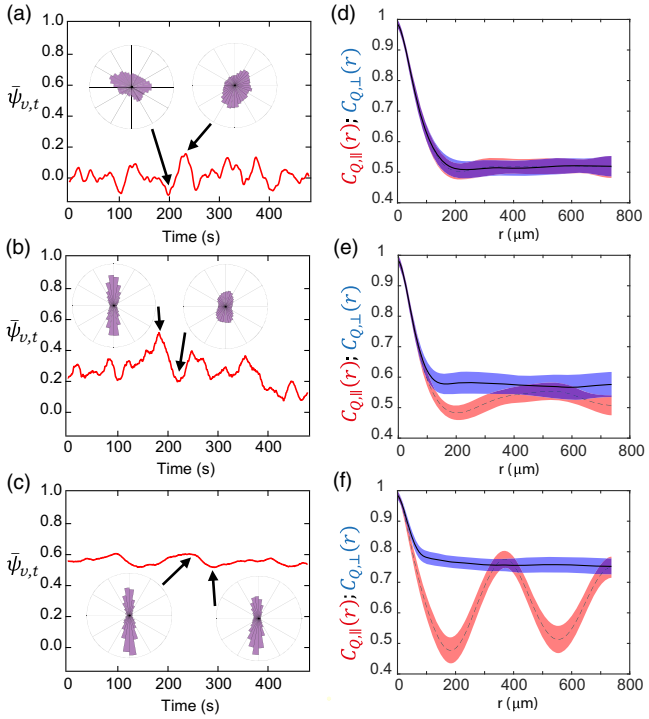

FIG. 4. Onset of the alignment transition. (a)–(c) Temporal evolution of the spatially averaged velocity order parameter $\bar{\psi}_{v,t}$. The insets correspond to the instantaneous distribution of velocity orientations at the times indicated by arrows. (d)–(f) Temporal evolution of the perpendicular to $\vec{H}$ (blue trace) and parallel to $\vec{H}$ (red trace) spatial correlation of the tensorial order parameter of the active nematic, $\mathbb{Q}$. The width of the bands are standard deviation around the time average. Data correspond to a decreasing temperature ramp at 33.60 °C (a),(d), 33.47 °C (b),(e), and 33.40 °C (c),(f).

interesting signatures of the alignment transition (Fig. 4). We do this analysis by computing the spatial correlations of the nematic tensorial order parameter, $\mathbb{Q} = 2S(\mathbf{nn} - 1/2\mathbb{1})$ [19], where S is the scalar nematic order parameter and $\mathbf{n}$ is the nematic director field. These correlations quantify the extent and decay of the AN orientational order and its emergence during the alignment transition. In Figs. 4(d)–4(f), we measure separately the correlations in the direction parallel, $C_{Q,\parallel}(r)$ (red traces), and perpendicular, $C_{Q,\perp}(r)$ (blue traces), to the applied magnetic field.

In the turbulent regime [Fig. 4(a)], thick AN bundles adopt random orientations but with a persistence length in excess of 100 μm [Fig. 2(a)]. The finite size of the field of view (around 10 times the persistence length), results in temporal oscillations of $\bar{\psi}_{v,t}$, rather than the steady state value $\bar{\psi}_{v,t} = 0$ that should correspond to a spatially isotropic state. The distribution of velocity orientations is quite isotropic in this regime, even when $\bar{\psi}_{v,t}$ fluctuates toward higher values [see inset in Fig. 4(a)]. The $\mathbb{Q}$-correlation curves overlap, consistently with the absence of anisotropy, and dropping their magnitude to around 0.5 at a distance corresponding to the coherence length of the unconstrained AN bundles [Fig. 4(d)].

In the aligned regime [Figs. 2(c) and 4(c)], there are also oscillations in $\bar{\psi}_{v,t}$, but these occur at higher mean values and their origin is more subtle than in the turbulent regime. Thick AN bundles self-organize into the antiparallel flow pattern described above [Fig. 1(d)]. The aligned bundles accumulate active stress that is released periodically in the form of bursts of bend instabilities perpendicular to the easy-flow direction that will span a certain fraction of the field of view [24]. These localized instabilities lower the instantaneous value of $\bar{\psi}_{v,t}$, which will gradually recover once the active filaments reorganize again along the easy-flow direction. In spite of these oscillations, active flows are clearly anisotropic at all times in the aligned regime [see inset in Fig. 4(c)]. We emphasize that we are using a low ATP concentration to minimize the magnitude of these oscillations (see Supplemental Material, Movie S3 [27] for an example of the clear oscillating dynamics seen in the aligned state at ten times higher ATP concentration). In this regime, the two $\mathbb{Q}$-correlation curves are clearly separated. $C_{Q,\perp}(r)$ drops to a steady-state value of around 0.78 at a distance equal to the coherence of the AN bundles within the aligned chevrons. Conversely, $C_{Q,\parallel}(r)$ has an oscillating behavior [Fig. 4(f)], with its maxima occurring at distances multiple of the chevron width, and its minima at odd multiples of the chevron half width.

With the chosen experimental conditions, oscillations in the order parameters have the highest amplitude during the transition regime [Fig. 4(b) and Supplemental Material, Fig. S5 and Movie S4 [27]], whose onset is evidenced by the emergence of spatial anisotropy upon sample cooling (Fig. 2). Similarly, the onset of the alignment transition can be clearly detected in Fig. 4(e), where the traces of $C_{Q,\perp}(r)$ and $C_{Q,\parallel}(r)$ are already distinguishable and do not overlap like in the turbulent regime. The trace of $\bar{\psi}_{v,t}$ contains large amplitude oscillations, whose minima coincide with episodes of low anisotropy in the velocity field, while the maxima arise when velocity anisotropy is high [see insets in Fig. 4(b)]. We have ruled out noise from the temperature controller as the source of these oscillations by comparing the temporal fluctuations of temperature with the oscillations in $\bar{\psi}_{n,t}$. Indeed, while the former have a frequency of the order of 1 Hz and are followed by the 8CB layer, the latter are at least 50 times slower, indicating that these oscillations are intrinsic to the AN, and not following fluctuations either on the temperature controller or on the 8CB layer (see Supplemental Material, Fig. S6 [27]).

The reported oscillating behavior in the transition region evidences both intermittent dynamics of the order parameter and spatial coexistence of turbulent and aligned regions, a signature that this transition is, in fact, discontinuous or first order. The abrupt, yet continuous change in

$\bar{\psi}_v$ reported in Fig. 3 could, nevertheless, be compatible with a continuous transition between the aligned and disordered regimes. A continuous transition, however, would be inconsistent with the temporal alternation between high anisotropy and low anisotropy configurations that coincide with large-amplitude oscillations in $\bar{\psi}_{v,t}$ and $\bar{\psi}_{n,t}$ in the transition region [Fig. 4(b) and Supplemental Material, Movie S4 [27]].

Spatial coexistence is evidential by the formation, during the alignment transition, of localized ordered regions that remain in that state for a period of time. When their span is comparable to the field of view, $\bar{\psi}_{v,t}$ attains a local maximum. While identifying these aligned domains may be difficult from the fluorescence micrographs, they are more easily revealed when considering the velocity field (see Supplemental Material, Fig. S7 and Movie S4 [27]). Conversely, when most of the field of view is in the disordered state, $\bar{\psi}_{v,t}$ attains a local minimum. Finally, when small ordered and disordered domains coexist, they average out in the field of view, and $\bar{\psi}_{v,t}$ features only small amplitude fluctuations about its mean value, and the complex nature of this dynamic transition is not readily apparent. In Supplemental Material, Fig. S7 [27], we have identified some instances of the spatial coexistence between aligned and disordered regions during the alignment transition. In those examples, we indicate the contrasted instantaneous value of $\bar{\psi}_{v,t}$ measured inside and outside the aligned regions.

The fact that this dynamic transition is discontinuous, yet it exhibits a continuous change in the order parameter, could be interpreted as a smoothening due to finite size effects. This is not unusual in active matter, where the number of constituent building blocks is typically small, always far from atomic or molecular systems where phase transitions are usually studied. On the other hand, it is known that the nematic phase of thermotropic liquid crystals (LCs) features pretransitional effects where regions with smecticlike order, or cybotactic groups, emerge close to $T_{\text{N-Sm}A}$ [29]. This is likely to have an impact on the rheology of the mesophase, and could justify that AN alignment starts at temperatures slightly above $T_{\text{N-Sm}A}$. In addition, coupling with the flowing AN results in energy injection into the LC at a broad range of length scales [30]. This may trigger anomalously high fluctuations in the Sm*A* phase close to the transition temperature, and could justify that the AN alignment transition is not completed until the temperature is slightly below $T_{\text{N-Sm}A}$.

In spite of the above considerations, and although one could think of a coupling between the orientational state and the triggered flows in the passive smectic, similar to elastic and viscous interactions analyzed in conventional LC [31], we do not expect a significant modification of the thermodynamics of the *N*-Sm*A* phase transition in 8CB, which is know to remain second order under flow conditions [32,33]. In fact, we have monitored such transition by observing the aqueous-oil interface under crossed polarizers, and have found no significant difference when the process takes place in contact with a fully active layer (Supplemental Material, Movie S5 [27]) or after deactivation the system (Supplemental Material, Movie S6 [27]).

In the reported experiments, both the passive (8CB) and active (AN) subsystems change their inherent symmetries at the crossover temperature, but in a very different way and affecting very different length scales. While 8CB mesogens gain spatial correlations in transitioning from the positionally disordered nematic arrangement to the layered configuration of the smectic-*A* phase, the concurrent AN flows change from the isotropic turbulent to an aligned, quasilaminar regime, at a much larger length scale.

In conclusion, we have experimentally studied an alignment transition in a microtubule-kinesin active nematic, a particular type of wet active matter. The alignment of the normally turbulent active flow is driven by the phase transition of a viscously coupled molecular liquid crystal from the nematic to the smectic phase. While the latter is known to be a continuous process, our observations suggest that the transition to the oriented state of the active nematic is discontinuous. Experimentally, this is evidenced by the spatial coexistence of disordered and aligned regions, and by the constant-temperature oscillation of the relevant order parameters between values corresponding to the ordered and disordered states. Future work to unravel the origin of the fascinating difference between transitions in the active and in the passive coupled phases calls for new developments in the statistical physics of active matter. In a broader context, our result should trigger further attempts to study alignment transitions in other wet active systems and should elicit a revision of existing models to include both dry and wet active matter in a universal treatment of alignment transitions.

The authors are indebted to the Brandeis University MRSEC Biosynthesis facility for providing the tubulin. We thank M. Pons, A. LeRoux, and G. Iruela (Universitat de Barcelona) for their assistance in the expression of motor proteins. O. B. acknowledges a Joan Oró FI fellowship (2023 FI-3 00065) by the Secretariat of Universities and Research of the Department of Research and Universities of the Generalitat of Catalonia and the European Social Plus Fund. O. B., J. I.-M., and F. S. acknowledge funding from MCINN/AEI/10.13039/501100011033/FEDER, UE (Grants No. PID2019–108842GB-C22 and No. PID2022-137713NB-C21). J. N. and A. F-N. acknowledge funding from MCINN/AEI/10.13039/501100011033/FEDER, UE (Grant No. PID2021-122369NB-100). Brandeis University MRSEC Biosynthesis facility is supported by NSF MRSEC 2011846. O. B. acknowledges a travel fund and scholarship from Munich Institute for Astro-, Particle and BioPhysics (MIAPbP), which is funded by the Deutsche

Forschungsgemeinschaft (DFG, German Research Foundation) under Germany´s Excellence Strategy—EXC-2094—390783311. The authors acknowledge helpful discussions with H. Chaté.

*f.sagues@ub.edu
†jignes@ub.edu

[1] S. Ramaswamy, The mechanics and statistics of active matter, Annu. Rev. Condens. Matter Phys. **1**, 323 (2010).
[2] M. C. Marchetti, J. F. Joanny, S. Ramaswamy, T. B. Liverpool, J. Prost, M. Rao, and R. A. Simha, Hydrodynamics of soft active matter, Rev. Mod. Phys. **85**, 1143 (2013).
[3] F. Sagués, *Colloidal Active Matter: Concepts, Experimental Realizations, and Models*, 1st ed. (CRC Press, Boca Raton, FL, 2022).
[4] M. E. Cates and J. Tailleur, Motility-induced phase separation, Annu. Rev. Condens. Matter Phys. **6**, 219 (2015).
[5] M. N. van der Linden, L. C. Alexander, D. G. A. L. Aarts, and O. Dauchot, Interrupted motility induced phase separation in aligning active colloids, Phys. Rev. Lett. **123**, 098001 (2019).
[6] D. Geyer, D. Martin, J. Tailleur, and D. Bartolo, Freezing a flock: Motility-induced phase separation in polar active liquids, Phys. Rev. X **9**, 031043 (2019).
[7] H. Chaté, Dry aligning dilute active matter, Annu. Rev. Condens. Matter Phys. **11**, 189 (2020).
[8] T. Ihle, Invasion-wave-induced first-order phase transition in systems of active particles, Phys. Rev. E **88**, 040303(R) (2013).
[9] A. P. Solon and J. Tailleur, Revisiting the flocking transition using active spins, Phys. Rev. Lett. **111**, 078101 (2013).
[10] M. E. Cates, D. Marenduzzo, I. Pagonabarraga, and J. Tailleur, Arrested phase separation in reproducing bacteria creates a generic route to pattern formation, Proc. Natl. Acad. Sci. U.S.A. **107**, 11715 (2010).
[11] J. Schwarz-Linek, C. Valeriani, A. Cacciuto, M. E. Cates, D. Marenduzzo, A. N. Morozov, and W. C. Poon, Phase separation and rotor self-assembly in active particle suspensions, Proc. Natl. Acad. Sci. U.S.A. **109**, 4052 (2012).
[12] M. L. Blow, S. P. Thampi, and J. M. Yeomans, Biphasic, lyotropic, active nematics, Phys. Rev. Lett. **113**, 248303 (2014).
[13] V. Soni, E. S. Bililign, S. Magkiriadou, S. Sacanna, D. Bartolo, M. J. Shelley, and W. T. M. Irvine, The odd free surface flows of a colloidal chiral fluid, Nat. Phys. **15**, 1188 (2019).
[14] R. Adkins, I. Kolvin, Z. You, S. Witthaus, M. C. Marchetti, and Z. Dogic, Dynamics of active liquid interfaces, Science **377**, 768 (2022).
[15] A. M. Tayar, F. Caballero, T. Anderberg, O. A. Saleh, M. Cristina Marchetti, and Z. Dogic, Controlling liquid-liquid phase behaviour with an active fluid, Nat. Mater. **22**, 1401 (2023).
[16] R. Assante, D. Corbett, D. Marenduzzo, and A. Morozov, Active turbulence and spontaneous phase separation in inhomogeneous extensile active gels, Soft Matter **19**, 189 (2023).
[17] S. Bhattacharyya and J. M. Yeomans, Phase separation driven by active flows, Phys. Rev. Lett. **130** (2023).
[18] T. Sanchez, D. T. Chen, S. J. DeCamp, M. Heymann, and Z. Dogic, Spontaneous motion in hierarchically assembled active matter, Nature (London) **491**, 431 (2012).
[19] A. Doostmohammadi, J. Ignés-Mullol, J. M. Yeomans, and F. Sagués, Active nematics, Nat. Commun. **9**, 3246 (2018).
[20] L. Giomi, Geometry and topology of turbulence in active nematics, Phys. Rev. X **5**, 031003 (2015).
[21] J. Urzay, A. Doostmohammadi, and J. M. Yeomans, Multi-scale statistics of turbulence motorized by active matter, J. Fluid Mech. **822**, 762 (2017).
[22] B. Martínez-Prat, J. Ignés-Mullol, J. Casademunt, and F. Sagués, Selection mechanism at the onset of active turbulence, Nat. Phys. **15**, 362 (2019).
[23] P. Guillamat, J. Ignés-Mullol, S. Shankar, M. C. Marchetti, and F. Sagués, Probing the shear viscosity of an active nematic film, Phys. Rev. E **94**, 060602(R) (2016).
[24] P. Guillamat, J. Ignés-Mullol, and F. Sagués, Control of active liquid crystals with a magnetic field, Proc. Natl. Acad. Sci. U.S.A. **113**, 5498 (2016).
[25] P. Guillamat, J. Ignés-Mullol, and F. Sagués, Taming active turbulence with patterned soft interfaces, Nat. Commun. **8**, 564 (2017).
[26] K. Thijssen, L. Metselaar, J. M. Yeomans, and A. Doostmohammadi, Active nematics with anisotropic friction: The decisive role of the flow aligning parameter, Soft Matter **16**, 2065 (2020).
[27] See Supplemental Material at http://link.aps.org/supplemental/10.1103/PhysRevLett.132.228302 for supplementary figures and videos.
[28] P. Oswald and P. Pieranski, *Nematic and Cholesteric Liquid Crystals: Concepts and Physical Properties Illustrated by Experiments* (Taylor & Francis, London, 2005).
[29] P. Oswald and P. Pieranski, *Smectic and Columnar Liquid Crystals: Concepts and Physical Properties Illustrated by Experiments* (Taylor & Francis, Boca Raton, FL, 2006).
[30] R. Alert, J.-F. Joanny, and J. Casademunt, Universal scaling of active nematic turbulence, Nat. Phys. **16**, 682 (2020).
[31] A. Sengupta, S. Herminghaus, and C. Bahr, Liquid crystal microfluidics: Surface, elastic and viscous interactions at microscales, Liq. Cryst. Rev. **2**, 73 (2014).
[32] C. R. Safinya, E. B. Sirota, and R. J. Plano, Nematic to smectic-*A* phase transition under shear flow: A nonequilibrium synchrotron x-ray study, Phys. Rev. Lett. **66**, 1986 (1991).
[33] T. Yamamoto, Y. Nagae, T. Wakabayashi, T. Kamiyama, and H. Suzuki, Calorimetry of phase transitions in liquid crystal 8CB under shear flow, Soft Matter **19**, 1492 (2023).